MATERIALS CHEMISTRY FRONTIERS

RESEARCH ARTICLE

View Article Online
View Journal | View Issue

Cite this: *Mater. Chem. Front.*, 2023, **7**, 1082

The fluorescence quenching mechanism of tetrazine-functionalized fluorogenic labels with integrated π-conjugations: internal conversion to a dark state†

Tianruo Shen,[a] Wenda Zhang,[ab] Priya Yadav,[a] Xiao Wei Sun[b] and Xiaogang Liu*[a]

Received 6th December 2022,
Accepted 18th January 2023

DOI: 10.1039/d2qm01264b

rsc.li/frontiers-materials

Tetrazine-based fluorogenic labels have been extensively applied to the studies of living systems due to their excellent selectivity, rapid reaction kinetics, and unique fluorogenicity. However, the fluorescence quenching mechanism in many precursor dyes remains controversial, impeding rational molecular engineering to optimize their fluorescence enhancement ratios. Herein, employing quantum chemical calculations, we established a quenching mechanism – internal conversion to a dark state (ICDS), to rationalize the fluorogenicity in tetrazine-functionalized labels with integrated π-conjugations. We show that the ICDS efficiency is negatively correlated with the energy gap between these labels' first excited state (the dark state) and the second excited state (the bright state). Based on this correlation, we further proposed molecular design strategies for developing biocompatible long-wavelength fluorophores with improved fluorogenicity.

Introduction

In the past few decades, bioorthogonal reactions have been widely deployed for tagging and monitoring various biomolecules and organelles in living systems with excellent biocompatibility.[1–7] Among the multitudinous bioorthogonal reactions, the inverse electron-demand Diels–Alder (iEDDA) reaction based on the tetrazine ligation stands out because of its favorable chemoselectivity, rapid reaction kinetics, and unique fluorogenicity.[8–12] Tetrazine-derived fluorogenic labels are weak or non-emissive. Enhanced fluorescence signals are released by removing tetrazine groups upon the iEDDA reactions with dienophiles or the [4+1] cycloaddition reactions with isocyanides.[13–16] This fluorogenicity associated with these reactions minimizes interference from background emissions and is highly desirable in bioimaging applications.[17–25] Accordingly, considerable research efforts have been devoted to developing tetrazine-functionalized labels with outstanding fluorescence enhancement (FE) ratios.[26–28] To aid the rational development of such fluorogenic dyes, it is critical to understand the molecular origins of fluorogenicity in tetrazine-functionalized fluorescent labels.

The molecular structures of tetrazine-functionalized fluorogenic labels can be broadly classified into three types based on the distance between the tetrazine fragment and the fluorophore. In the first type, tetrazine is attached to the fluorophore through a long linker, with a large distance between these two fragments (Scheme 1(a)).[29,30] Such compounds typically possess low to moderate FE ratios. In the second type, the lengths of the linkers/spacers are significantly reduced, resulting in a short distance between the tetrazine moiety and the fluorophore (Scheme 1(a)).[31–34] It is worth highlighting that Wombacher and co-workers developed fluorogenic labels with a stacking conformation between the fluorophore and tetrazine, thus significantly minimizing their distance to <1 nm.[32] Such labels usually exhibit moderate to high FE ratios. In the last type, tetrazine is directly "fused" to the fluorophore, resulting in an integrated π-conjugation (Scheme 1(a) and Fig. 1).[35–38] In other words, the tetrazine fragment becomes a part of the resulting fluorophore. In such cases, the distances between the fluorophore and the tetrazine moiety become approximately zero. Such fluorogenic labels afford moderate to high fluorescence turn-on ratios across the visible-near-infrared (NIR) spectrum.

In parallel with developing these tetrazine-functionalized labels, several mechanisms have been proposed to rationalize their unique fluorogenicity. Choi *et al.* summarized that the low

[a] *Science, Mathematics and Technology Cluster, Singapore University of Technology and Design, 8 Somapah Road, Singapore 487372, Singapore. E-mail: xiaogang_liu@sutd.edu.sg*
[b] *Institute of Nanoscience and Applications and Department of Electrical and Electronic Engineering, Southern University of Science and Technology, Shenzhen 518055, China*

† Electronic supplementary information (ESI) available. See DOI: https://doi.org/10.1039/d2qm01264b

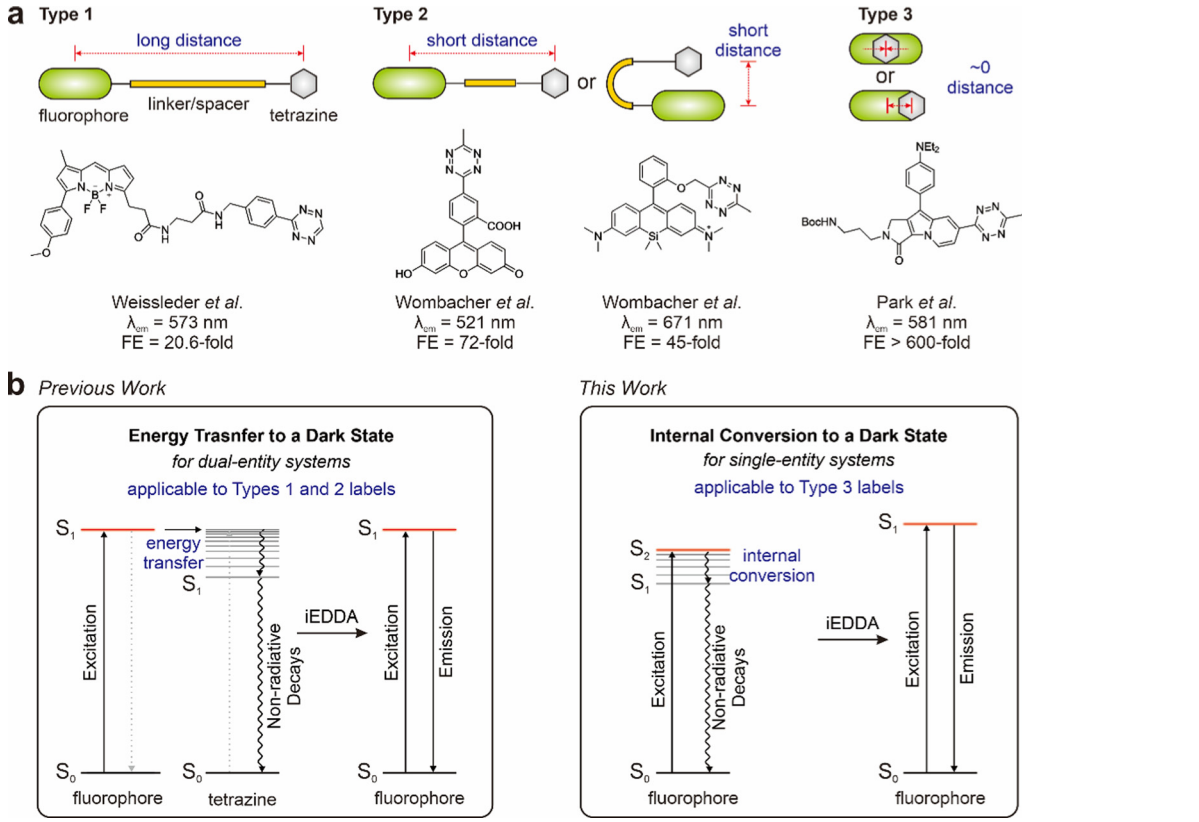

Scheme 1 (a) Schematic illustrations of types 1, 2 and 3 of tetrazine-based fluorogenic labels with representative molecular structures.[30–32,35] The insets show the peak emission wavelengths (λ_{em}) and fluorescence enhancement (FE) ratios upon iEDDA reactions. (b) Illustrations of the energy transfer to a dark state (ETDS; left) and internal conversion to a dark state (ICDS; right) working mechanisms for the tetrazine-based fluorogenic labels.

background emissions of tetrazine-modified precursors are attributed to electronic energy transfer (EET) from the fluorophore to the tetrazine fragment.[39] EET could be further classified into (1) Förster resonance energy transfer-type (FRET-type) EET,[40] (2) Dexter energy transfer-type (DET-type) EET,[41] and (3) through-bond energy transfer-type (TBET-type) EET.[42] FRET is typically applicable when the fluorophore–tetrazine distance is greater than 1 nm, while DET dominates when this distance becomes less than 1 nm.[43–45] No effective way is available to distinguish TBET from FRET/DET. In the so-called TBET dyes, the employment of rigid and conjugated linkers probably enhances the efficiency of energy transfer.[42] To this end, Liu and co-workers proposed a unified fluorescence quenching mechanism: energy transfer to a dark state (ETDS; Scheme 1(b) left) of tetrazine-based fluorogenic labels.[33] ETDS highlights a dark state generated by the n–π* transition induced by the tetrazine fragment (the energy acceptor), which leads to fluorescence quenching in tetrazine-functionalized labels. Liu *et al.* further showed that the FE ratio is closely related to two major factors: (1) the energy difference between the bright state [the first excited state (S_1) of the fluorophore fragment] and the dark state (S_1 of the tetrazine moiety; $\Delta E = E_{bright} - E_{dark}$), which correlates with the spectral overlap between the fluorophore and tetrazine fragments; and (2) the centroid distance between the tetrazine group and the fluorophore fragment. A large ΔE and a short centroid distance can improve fluorescence turn-on ratios. In addition to energy transfer, photon-induced electron transfer (PET) could also occur between the fluorophore and the tetrazine fragment, resulting in fluorescence quenching.[28] During energy transfer (as well as electron transfer), the fluorophore and the tetrazine moieties act as two independent entities (*i.e.*, as a donor or an acceptor, respectively). ETDS (and PET) are thus only applicable to the first two types of tetrazine-functionalized labels, in which tetrazine and fluorophores are separated by a linker/spacer and possess two independent conjugated networks. In the third type of tetrazine-derived fluorogenic labels, the π-conjugation of tetrazine and the fluorophore becomes integrated and collectively forms a new dye. For instance, Kele and co-workers reported a series of coumarin-derived tetrazine-integrated chromophores with enhanced fluorescence turn-on ratios (>1000-fold).[36] Their computational results showed that tetrazine participated in the frontier molecular orbitals of the resulting chromophores. These chromophores could transit from the second excited state (S_2) to S_1 (a dark state) *via* internal conversion, subsequently returning to S_0 through non-radiative decays. However, in several other tetrazine-integrated fluorophores, the structure–property relationships of these dyes remain incomplete.[35,37] These results are critical to expediting the rational development of tetrazine-functionalized labels with improved fluorogenicity and wavelengths/colors.

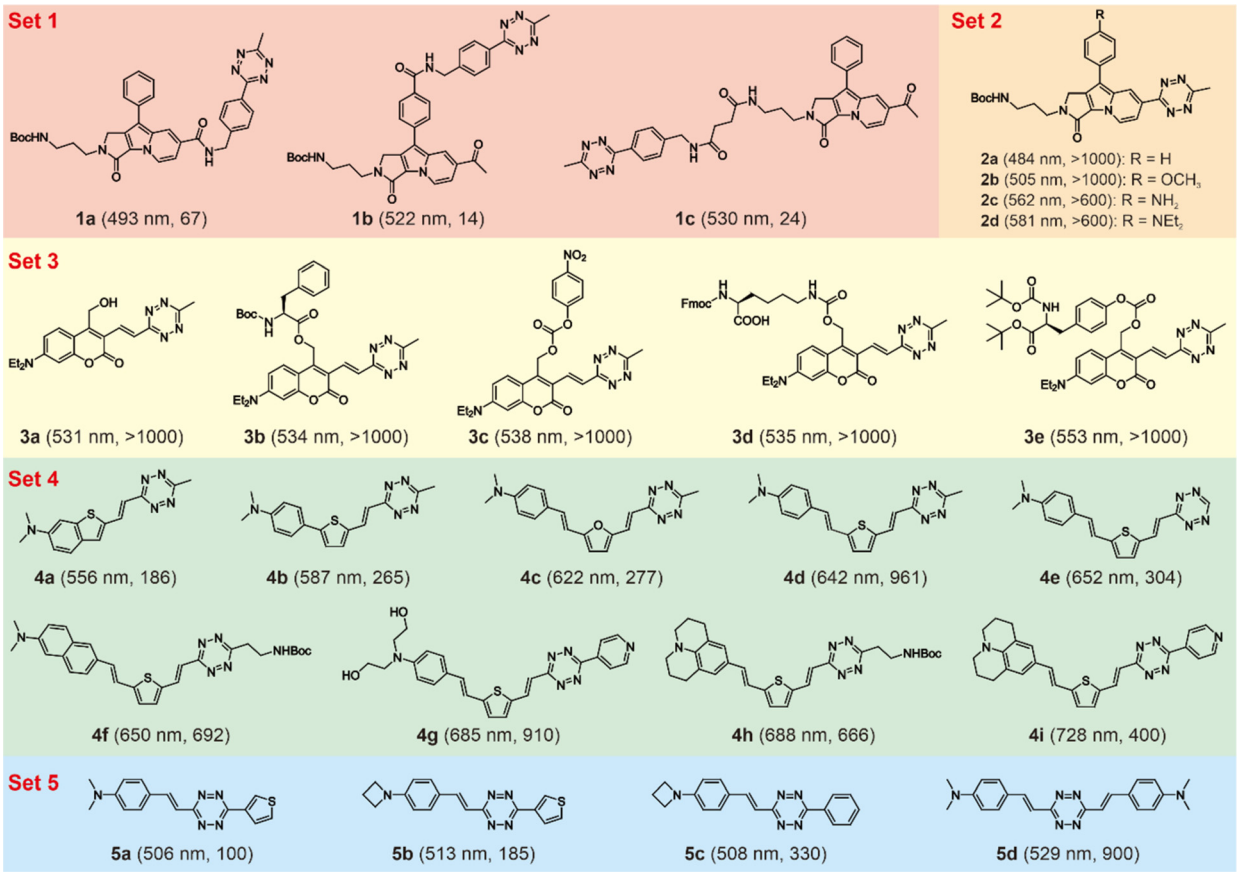

Fig. 1 Molecular structures of five sets of tetrazine-based fluorogenic dyes. The numbers in the brackets stand for λ_{em} and FE ratios, respectively. The experimental conditions are listed in Table S1 (ESI†).

In this work, we conducted detailed quantum chemical calculations to investigate the fluorescence quenching mechanism of tetrazine-functionalized fluorogenic labels with integrated π-conjugations (the third type) and study factors affecting the FE ratios of these labels (Fig. 1). Based on these results, we formalized a fluorescence quenching mechanism, namely, internal conversion to a dark state (ICDS) to rationalize the fluorogenicity of these labels. Furthermore, the ICDS was compared with the ETDS in detail (Scheme 1(b)). Guided by ICDS mechanisms, we further proposed several strategies to develop long-wavelength tetrazine-functionalized labels with large FE ratios.

Results and discussion

Formalization of the fluorescence quenching mechanism – internal conversion to a dark state

We started by comparing the electronic structures of two sets of tetrazine-functionalized fluorogenic dyes reported by Park and co-workers (Sets 1 and 2; Fig. 1).[35] In Set 1 molecules, tetrazine groups are linked to Seoul-Fluor (SF) *via* different linkers/spacers. The FE ratios of these labels after reacting with *trans*-cyclooctene (**TCO**) were moderate (14 to 67-fold). In contrast, tetrazine is directly attached to SF in four Set 2 labels. These dyes displayed significant FE ratios after the iEDDA reactions (>600-fold).

To rationalize the different FE ratios, we carried out quantum chemical calculations to optimize the geometries, and thereby retrieve the energy levels of various states and electronic structures with the corresponding oscillator strengths (f) of these two sets of dyes. It is worth mentioning that we conducted our calculation on two simplified molecules (**1a′** and **2a′**) and their products (**1a′-BCN** and **2a′-BCN**) after the iEDDA reaction with bicyclononyne (**BCN**; Fig. 2(a) and 3(a)). These simplified molecules are obtained by removing side chains in **1a** and **2a**, and this treatment does not affect the calculated optical properties of these molecules.[33]

Our results revealed that the S_1 photoexcitation of the tetrazine moiety is independent of the SF fragment in **1a′** (Fig. 2(a)). During the vertical excitation of **1a′**, the tetrazine moiety introduces a low-lying dark state ($S_{1,TZ}$), due to the forbidden n–π* transition (Fig. 2(b) and (c)). Photoexcitation to this dark state is accompanied by a negligible f value and a small charge transfer distance (d_{CT}) of 0.012 Å (Fig. 2(c)). d_{CT} quantifies the distance between the centroids of the electron and the hole involved during photoexcitation to a specific state, and a large d_{CT} indicates the substantial intramolecular charge transfer (ICT). Above this dark state ($S_{1,TZ}$), we observed a bright state (f = 0.4269) generated by the SF fragment ($S_{1,SF}$).

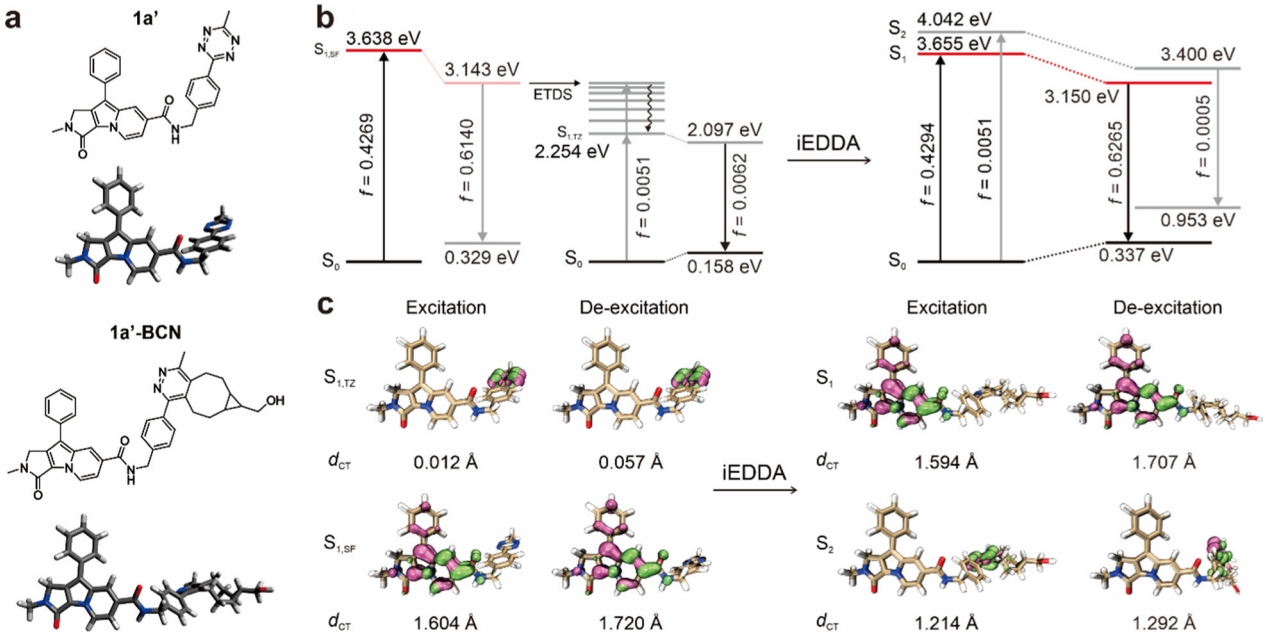

Fig. 2 (a) Molecular structures and optimized geometries, (b) energy levels of key states during the excitation and de-excitation processes, and (c) corresponding hole–electron distributions (mauve: hole; green: electron) with d_{CT} of **1a**′ and **1a**′**-BCN**.

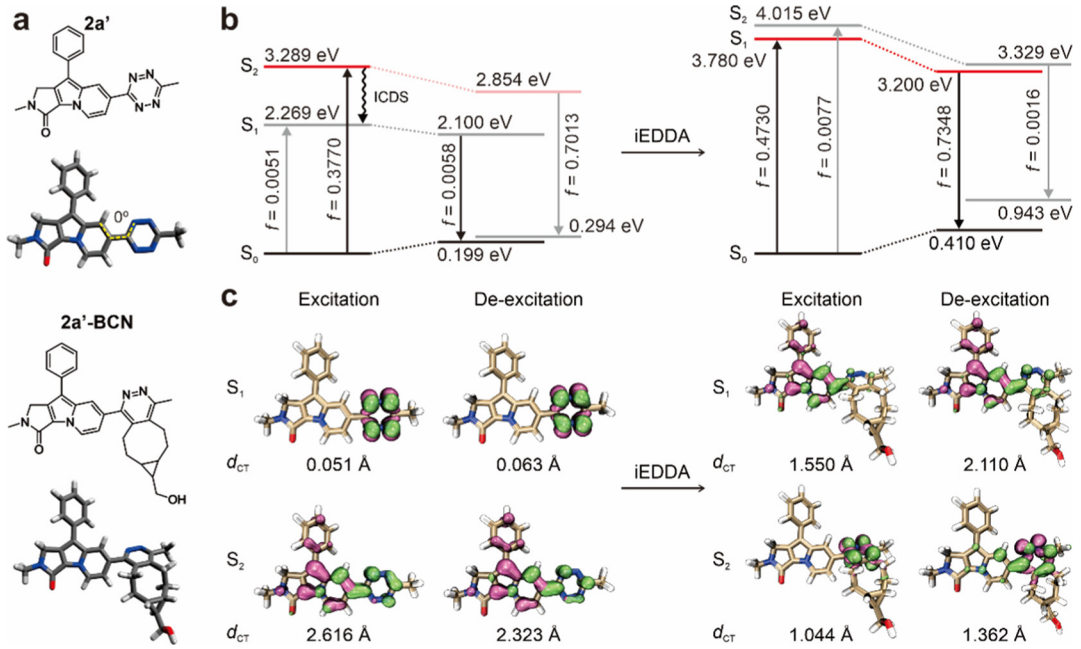

Fig. 3 (a) Molecular structures and optimized geometries, (b) energy levels of key states during the excitation and de-excitation processes, and (c) corresponding hole–electron distributions (mauve: hole; green: electron) with d_{CT} of **2a**′ and **2a**′**-BCN**.

This bright state corresponds to the π–π* transition in SF and displays an ICT characteristic with a large d_{CT} of 1.604 Å. $S_{1,SF}$ is 1.384 eV higher than $S_{1,TZ}$ during vertical excitation. Notably, the distribution of the frontier molecular orbitals (or electron/hole) of $S_{1,SF}$ and $S_{1,TZ}$ does not overlap but centralizes on the SF and tetrazine fragments, respectively (Fig. S1a and b, ESI†).

Hence, **1a**′ can be viewed as a dual-entity molecule consisting of two electronically independent fragments (tetrazine and SF, respectively). The dark state ($S_{1,TZ}$) remains more stable than the bright state ($S_{1,SF}$) during the de-excitation process (Fig. 2(b)). These energy levels suggest that energy transfer could take place from SF (the energy donor) to tetrazine (the energy acceptor), and subsequently dissipates as heat *via* the dark state and affords low background emissions. These results are consistent with the previously proposed ETDS model (Scheme 1(b), the left panel). After destroying the tetrazine

moiety *via* the iEDDA reaction, the low-lying dark state ($S_{1,TZ}$) is eliminated. $S_{1,SF}$ becomes the most stable excited singlet state in **1a′-BCN** with a considerable f value during excitation and de-excitation processes. Accordingly, **1a′-BCN** is highly emissive. The transformation from **1a′** to **1a′-BCN** thus affords a moderate FE ratio.

It is of note that the bright states in **1a′** and **1a′-BCN** are almost identical in terms of excitation energy and electron/hole distributions (Fig. 2(c) and Fig. S1b, ESI†). The reaction of tetrazine with **BCN** does not affect $S_{1,SF}$ much because SF and tetrazine are two independent entities in **1a′**. Hence, the calculated peak ultraviolet-visible (UV-vis) absorption wavelength (λ_{abs}) remained almost unchanged in both **1a′** and **1a′-BCN** (Fig. S2, ESI†). Indeed, experimental measurements also show that **1a** and its product possess the same λ_{abs} (375 nm),[35] since the dark state from tetrazine ($S_{1,TZ}$) does not contribute to UV-vis absorption.

We next performed similar calculations for **2a′** and **2a′-BCN** (Fig. 3). In **2a′**, tetrazine is directly attached to SF. The optimized geometry of **2a′** displayed excellent planarity, with a 0° dihedral angle between the tetrazine group and the SF fragment (Fig. 3(a)). Owing to the planar conformation and the uninterrupted π-conjugation between SF and tetrazine, we speculated that tetrazine might become a part of this "fused" fluorophore. Further quantum chemical calculations show that the n–π* transition (d_{CT} = 0.051 Å) of the tetrazine fragment still produced a low-lying dark state (S_1, f = 0.0051) during the vertical excitation of **2a′** (Fig. 3(b) and (c)). The energy level of the bright state (S_2, f = 0.3770) is 0.138 eV higher than that of S_1. It is of note that the electron/hole distributions of this bright state span across SF and tetrazine. The tetrazine fragment contributed 4.12% and 40.24% to the hole and electron distributions of **2a′**, respectively (Fig. S1c, ESI†). These results suggest that both SF and tetrazine participated in the π–π* transition of the bright state (Fig. 3(c)). This contrasts with **1a′**, where only SF is involved in the π–π* transition of the bright state.

These results suggested that tetrazine is both geometrically and electronically coupled to SF and becomes a part of this integrated fluorophore **2a′**. In other words, **2a′** is a single-entity molecule; the distance between tetrazine and the fluorophore essentially decreased to zero in this "fused" fluorophore. Indeed, due to this integrated π-conjugation system, the bright state in **2a′** displayed a lower vertical excitation energy (3.289 eV) in comparison to that of **1a′** (3.638 eV), corresponding to the redshifted λ_{abs} in the calculated spectra (Fig. S2, ESI†). The experimental data further corroborate this difference, showing that **2a** (415 nm) possesses a longer λ_{abs} in comparison to that of **1a** (375 nm).[35] These changes in the geometrical and electronic structures require revising the energy transition mechanism from S_2 (bright) to S_1 (dark) in **2a′**. The UV-vis absorption in **2a′** occurs mainly *via* the S_0–S_2 transition. It is worth highlighting that the subsequent relaxation from S_2 to S_1 in **2a′** should be classified as internal conversion, instead of energy transfer, in this single-entity molecule. Finally, **2a′** returns to S_0 *via* non-radiative decays, resulting in an extremely low fluorescence intensity (Fig. 3(a)).

After reacting with **BCN**, we found that the S_1 of the product **2a′-BCN** becomes a bright state with a large oscillator strength f (with a π–π* transition characteristic; Fig. 3(b)). This π–π* transition remains the most stable singlet excited state during both excitation and de-excitation processes, indicating that **2a′-BCN** is highly emissive. We also noted that this bright state in **2a′-BCN** (S_1) exhibits a higher excitation energy than that in **2a′** (S_2). This change is consistent with the blueshift in the UV-vis absorption spectra observed in Kim's experiments,[35] *i.e.*, λ_{abs} is blue-shifted from 415 nm in **2a** to 386 nm in its product. This change also confirms that tetrazine indeed becomes a part of the fluorophore in **2a′**; the iEDDA reaction with tetrazine would alter the conjugation of the fluorophore and thereby causes the spectral shift.

We tentatively denominated this new fluorescence quenching mechanism revealed in **2a′** (or **2a**) as internal conversion to a dark state (ICDS; Scheme 1(b) right). In an ICDS-based dye, the tetrazine fragment that generates the low-lying dark state resides within the fluorophore. This contrasts with ETDS, in which the tetrazine quencher is independent of the fluorophore. Due to different geometrical and electronic structures, the ICDS dye **2a** (>1000-fold) displays a much higher FE ratio than the ETDS dye **1a** (67-fold).[35] The outstanding fluorogenicity in **2a** prompted us to investigate more tetrazine-functionalized fluorogenic labels with integrated π-conjugations and understand the newly formalized ICDS mechanism.

Generalizability of the ICDS mechanism

To understand the general applicability of the ICDS mechanism, we modelled other 21 tetrazine-functionalized fluorogenic labels/photocages with integrated π-conjugations, including Set 2 reported by Park *et al.*,[35] Set 3 reported by Kele *et al.*,[36] Set 4 reported by the Wu group,[37] and Set 5 reported by Vrabel and co-workers (Fig. 1).[38] All these compounds were applied in the fluorogenic labelling of living cells. We also modelled their derivatives after the iEDDA reactions with **BCN** (Fig. 4 and Fig. S3–S14, ESI†). We calculated the relative energy levels (between the dark and bright states) during vertical excitation. We did not model the de-excitation processes. Our results in Fig. 2 and 3 and a previous study show that the relative energy orders of the bright and dark states remain unchanged during the excitation and de-excitation processes in reported fluorogenic dyes.[33] Ignoring the de-excitation process significantly minimized the computational load, especially in large-scale calculations, while the corresponding conclusions on the quenching mechanism remained the same.

To our delight, all the results demonstrated the same trend as established in **2a′** and **2a′-BCN** (Fig. 3, 4, and Fig. S7–S14, ESI†). Before bioorthogonal reactions, these fluorophores are co-planar with tetrazine with flat dihedral angles and expansive π-conjugations (*e.g.*, in **3a**, **4c**, **5a**, and **5d**; Fig. 4 top panels). The tetrazine fragment participated in the π–π* transition of the bright ICT state (S_2). To this end, we have quantified the contribution of the tetrazine fragment (as well as its residue after iEDDA reactions) to the electron/hole of the bright state. We noted that these fragments have a more considerable

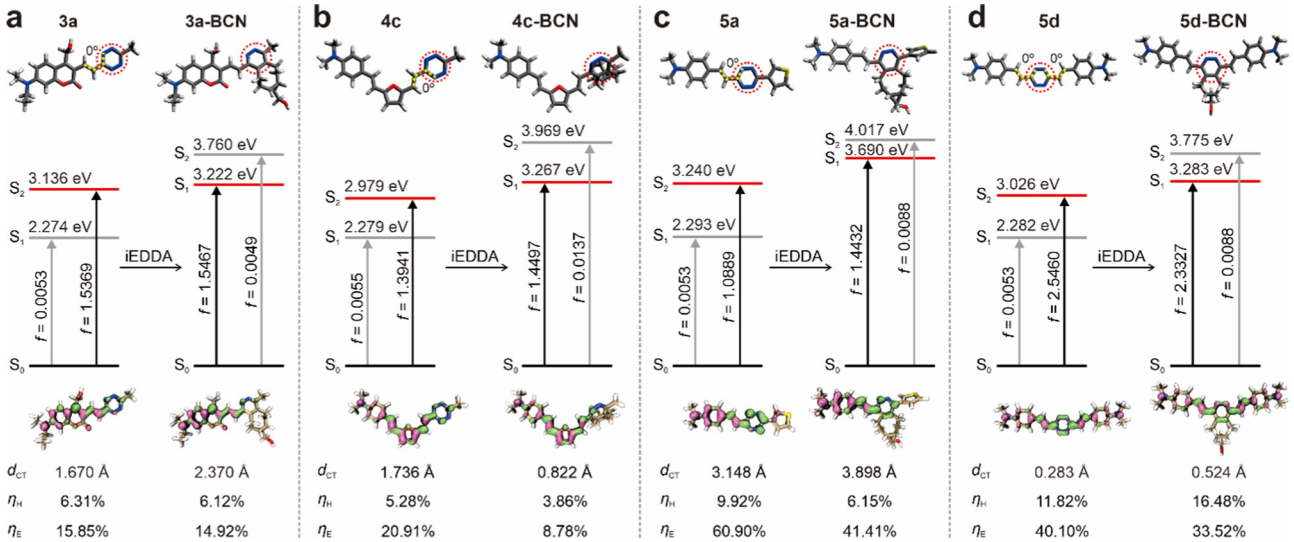

Fig. 4 Optimized ground-state geometries (top), energy levels of different vertical excitation states (middle), and corresponding hole–electron distributions (mauve: hole; green: electron) with d_{CT}, fragment contributions to the hole (η_H) and the electron (η_E) by highlighted fragments (red circles in Fig. 4(a)) of (a) **3a**, (b) **4c**, (c) **5a**, and (d) **5d** before and after reacting with **BCN**.

contribution in electrons than that in holes, corroborating the electron-withdrawing nature of the tetrazine fragment. Below the bright S_2 state, a low-lying dark state induced by the n–π* transition of the tetrazine group (S_1) exists in each precursor (Fig. 4 and Fig. S7–S14, ESI†), enabling internal conversion from S_2 to S_1 and thereby quench fluorescence *via* the dark state.

Contrarily, the alteration of tetrazine *via* the iEDDA reactions removes the low-lying n–π* dark state. In the resulting fluorophores, the S_0 to S_1 photoexcitation is dominated by the bright π–π* transition of the main fluorescent skeletons (with large f values; Fig. 4 and Fig. S7–S14, ESI†). This low-lying bright state turns on bright fluorescence and endows these compounds with large FE ratios. Once again, we noted that the bright states (S_1) in the resulting fluorophores have higher excitation energy than those of the precursor (S_2). This change corroborates that tetrazine becomes a part of the fluorophores. As a result, the reactions with tetrazine affect the excitation energy of dyes. These results demonstrate that ICDS applies to a wide range of chemical families of fluorophores.

The ΔE dependence of the ICDS mechanism

The general applicability of ICDS encouraged us to investigate its dependence on ΔE ($\Delta E = S_{2,bright} - S_{1,dark}$). In ICDS-based dyes, we do not expect any strong dependence on d (the distance between the fluorophore and the tetrazine fragments) because tetrazine becomes a part of the fluorophore, and d reduces to ~0. Instead, the rapid internal conversion from S_2 to S_1 should escalate as ΔE decreases (the energy gap law). This enhanced ICDS from S_2 to S_1, in turn, affords low background emissions and large FE ratios upon iEDDA reactions.

To verify this understanding, we compared two types of tetrazine-functionalized fluorogenic labels. Group I includes nine molecules reported by Wombacher *et al.* (Fig. S15, ESI†).[31] In these dual-entity molecules (type 2), tetrazine groups are electronically decoupled from the main fluorophores. Their fluorogenicity mechanism can be described by the ETDS model.[33] Group II covers nine compounds reported by Wu *et al.* (Set 4 in Fig. 1).[37] These single-entity dyes are of type 3, in which the tetrazine fragment becomes a part of the fluorophore. Their working mechanism is based on ICDS. We selected data from the same group (for groups I and II, respectively) to minimize variations in experimental conditions. Under this consideration, only Wu's work provided enough fluorophores with varied UV-vis absorption and emission peaks to establish the correlation. It is noted that the turn-on ratio is reported as a range (*e.g.*, >600-fold) instead of an exact value in several reports,[35,36] and we thus did not select and analyze these data.

These two groups of dyes display opposite FE-ΔE correlations. Group I exhibit a positive correlation ($r = 0.9810$) between the calculated ΔE values and the natural logarithm of experimental FE ratios (lnFE; Fig. 5(a) left and Table S2, ESI†). Given that the energy level of the dark state (S_1) remains unchanged and the Stokes shifts of Group I compounds are very small (~20 nm), a small ΔE corresponds to a low energy level of the bright state and thus a longer λ_{em}. Therefore, we also note that lnFE exhibited an excellent negative linear correlation with λ_{em} ($r = -0.9833$; Fig. 5(a) right and Table S2, ESI†). We have rationalized these correlations using the overlap between the fluorophore's emission spectrum and tetrazine's UV-vis absorption spectrum. A high ΔE value (or a short λ_{em}) reflects a sizeable spectral overlap (with the higher excited states of tetrazine), thus enabling more efficient energy transfer to tetrazine, weak background emission, and more excellent FE ratios upon subsequent iEDDA reactions.

Conversely, in Group II compounds, we noted that experimental lnFE and calculated ΔE demonstrated a negative correlation ($r = -0.6210$), while experimental lnFE is positively

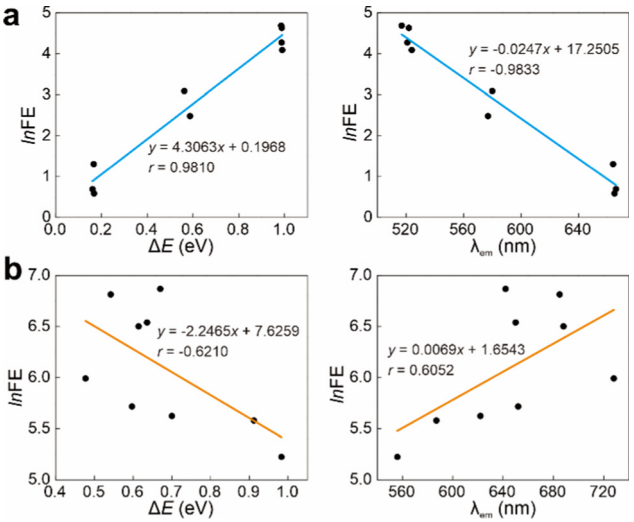

Fig. 5 The relationships between the lnFE and ΔE (left panels)/λ_{em} (right panels) of the products reported by (a) Wombacher *et al.*[31] and (b) Wu *et al.*[37] The insets show the best linear fitting equation with a correlation coefficient (*r*). Note that the ETDS governs the working mechanisms of dyes in (a) and in comparison to ICDS in (b).

correlated λ_{em} to (r = 0.6052; Fig. 5(b) and Table S3, ESI†). These correlation coefficients are moderate and probably affected by many factors other than ICDS (*e.g.*, molecular aggregations of NIR dyes). Yet, the contrast between Groups I (ETDS) and II (ICDS) is evident. The increasing FE ratios with the reduction of ΔE (or the increase of λ_{em}) corroborate the enhanced internal conversion rates (to the dark state) in long-wavelength ICDS fluorophores. Indeed, the absolute value of r in Group II compounds is much lower than that in Group I. This difference could be due to several factors: (1) the ΔE values are retrieved based on the S_2–S_1 energy gap during vertical excitation. In Group I compounds, the geometry relaxation and related reorganization energy are small, as reflected by the small Stokes shifts (~20 nm) in xanthene-based dyes or derivatives.[31] Hence, the vertical excitation approximation is "accurate" even when describing energy transfer from adiabatic excited states (of the energy donors). In Group II molecules, the push–pull effect is strong, and geometry relaxation becomes intensified, as shown by the large Stokes shifts (~200 nm).[37] Internal conversion could occur at any geometries between the Franck–Condon (FC) and adiabatic excited states. The approximation using vertical excitation energy (based on the FC state) to calculate ΔE becomes less ideal. (2) Compounds in Group I generally possess high quantum yields (QYs; ~0.30 on average; Table S2, ESI†),[31] while the QYs of Group II compounds are much lower (~0.18 on average; Table S3, ESI†).[37] The low quantum yield (after iEDDA reactions) suggests that the other non-radiative decay process (*i.e.*, twisting and rotations) could also affect the fluorogenicity in addition to ICDS. (3) These correlation coefficients could also be affected by other factors (*e.g.*, molecular aggregations of NIR dyes).

Overall, we noted that ICDS dyes (lnFE > 5) offered improved FE ratios than ETDS dyes (lnFE < 5). The same trend is also observed in Park's experiments,[35] as shown by the different FE ratios between Set 1 (ETDS) and Set 2 (ICDS) dyes (Fig. 1). This contrast in FE ratios is particularly stark in the long wavelength region (*e.g.*, $\lambda_{em} \geq 550$ nm; Fig. 5(b)). The FE ratio in these fluorogenic dyes largely depends on the background emission intensities.[28,30,33] A large rate of ICDS/ETDS facilitates the quenching of fluorescence and results in low background emissions, thus affording high FE ratios upon iEDDA reactions. Considering that internal conversions between the excited states of the same molecular entity are typically faster than energy transfer between two molecular entities,[46–48] ICDS-based fluorogenic dyes usually afford higher turn-on ratios.

Potential design strategies for developing ICDS-based fluorogenic labels with enhanced bathochromic shifts

Fluorophores of long wavelengths are essential in bioimaging applications to reduce phototoxicity, minimize interference from biological autofluorescence, and enhance penetration depths.[49–53] Additionally, large FE ratios of fluorogenic dyes improve signal-to-noise ratios during bioimaging. Given that ICDS affords long-wavelength fluorogenic dyes with excellent FE ratios, we next investigated potential molecular design strategies that utilize IDCS and afford bathochromic shifts in tetrazine-functionalized fluorogenic labels with integrated π-conjugations. Two frequently employed strategies to bathochromically shift the $\lambda_{abs}/\lambda_{em}$ of organic dyes were explored including expanding the π-conjugation and incorporating quinoidal structures.[54–60]

Strategy 1: expanding the π-conjugation. Based on **3a**, we introduced another coumarin fragment to form **3e** (Fig. 6(a) and Fig. S16, ESI†). The molecular structures of **3a** and **3e** are planar with an integrated conjugation between coumarins and tetrazine fragments (Fig. 4 and Fig. S16a, ESI†). In comparison to **3a**, compound **3e** exhibits an expanded π-conjugation network (Fig. 6(b)), resulting in bathochromic shifts in the $\lambda_{abs}/\lambda_{em}$ of the bright state (Fig. 6(c)). Moreover, the tetrazine group in **3e** showed enhanced contributions to the hole/electron distributions than that in **3a** (Fig. 6(b)). For instance, 8.70% of the hole and 25.46% of electron distributions in the bright state of **3e** are centralized in the tetrazine group (Fig. 6(b)). In **3a**, the tetrazine moiety only contributed 6.31% to the hole and 15.85% to the electron distributions, respectively.

Notably, the dark state S_1 in **3e** remains below the bright state (S_2) with a reduced ΔE of 0.549 eV compared to ΔE = 1.042 eV in **3a** during vertical excitation (Fig. 6(d) and Fig. S16b, ESI†). The alignment of these states ensures ICDS, effectively turning off the fluorescence of **3e**. Upon removing the tetrazine group in **3e-BCN**, the bright state becomes S_1 during excitation (f = 2.5881) and emission (f = 2.6441), corroborating the excellent fluorogenicity of **3e**.

Strategy 2: exchanging the π-conjugation order to induce quinoidization. Quinoidization caused by exchanging the connection orders of different molecular fragments represents another potential method to enhance bathochromic shifts.[58,59] To this end, we changed the connection order in **4b** by switching the positions of the thiophene ring with the methane unit to

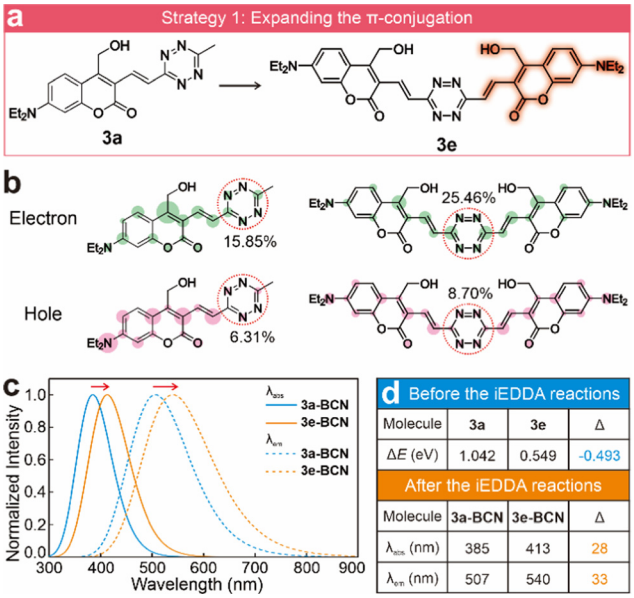

Fig. 6 (a) Schematic illustration of the design strategy 1. (b) Fragment contributions to the hole–electron distributions of **3a** (left) and **3e** (right). (c) Calculated UV-vis-NIR absorption/emission spectra and (d) calculated photophysical properties of **3a**/**3a-BCN** and **3e**/**3e-BCN** in ethanol.

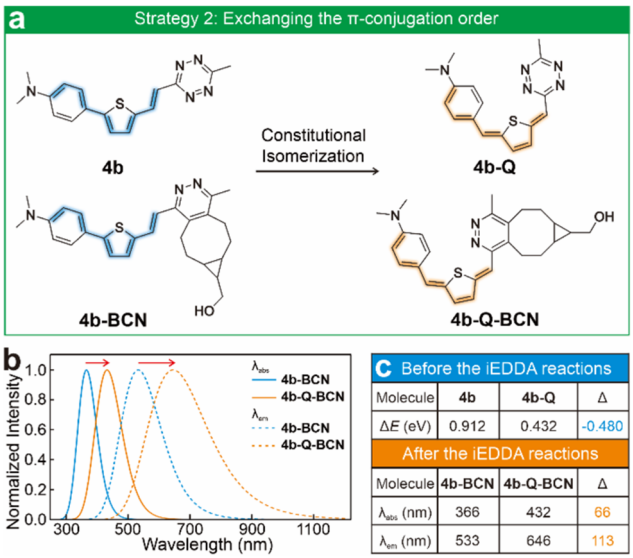

Fig. 7 (a) Schematic illustration of the design strategy 2. (b) Calculated UV-Vis-NIR absorption/emission spectra and (c) calculated photophysical properties of **4b**/**4b-BCN** and **4b-Q**/**4b-Q-BCN** in ethanol.

generate its constitutional isomer **4b-Q** (Fig. 7(a)). The bond length alternation (BLA) analysis along the highlighted fragments shows that **4b-Q**/**4b-Q-BCN** (with larger BLA values) displays a much stronger quinoidal characteristic than **4b**/**4b-BCN** does (with a smaller BLA value; Fig. 7(a) and Fig. S17, ESI†). Quinoidization could greatly enhance ICT in the ground state and reduce the HOMO–LUMO gap, thus affording a large redshift (Fig. S18–S21, ESI†).[57] Indeed, our calculations show that **4b-Q**/**4b-Q-BCN** displays much improved bathochromic shifts than **4b**/**4b-BCN** (Fig. 7(b)). In addition to redshifts, our calculations indicated that **4b-Q** possesses a reduced ΔE than **4b** does by 0.480 eV (Fig. 7(c) and Fig. S17, ESI† right). This reduced energy gap is conducive to expediting ICDS and increasing the FE ratio after the iEDDA reactions.

We successfully designed several tetrazine-based fluorogenic labels with long wavelengths and reduced ΔE. Such dyes are expected to possess enhanced FE ratios. More importantly, we hope that demonstrating these design strategies could inspire the development of highly creative ICDS molecules with long wavelengths and excellent fluorogenicity.

Limitations of the ICDS mechanism

The ICDS mechanism is likely disabled in fluorophores with $\lambda_{abs}/\lambda_{em}$ moving beyond ~700 nm. ICDS requires the presence of a low-lying dark state to quench fluorescence. As the spectra of fluorophores progressively move into the NIR region, the energy level of the bright state keeps dropping and could eventually fall below that of the dark state produced by tetrazine (~2.279 eV on average; Table S4, ESI†). In this scenario, ICDS becomes disabled and thus leads to strong background fluorescence and, subsequently, low FE ratios after iEDDA reactions. This limitation also applies to the ETDS mechanism.

To demonstrate this limitation of the ICDS mechanism, we linked the tetrazine fragment to two NIR fluorophores – Keio Fluors (KF) reported by Suzuki *et al.* and obtained two tetrazine-fused labels – **7a** and **7b** (Fig. 8(a), (c), and Fig. S22, ESI†).[61] Our computational results showed that **7a** displayed a stable, bright ICT state (S_1; 2.176 eV) with a large f value of 1.9004 during vertical excitation (Fig. 8(b)). The dark n–π* state generated by the tetrazine moiety is higher than the bright state by 0.134 eV. This low-lying bright state remains S_1 after geometric relaxation and could thus emit strong fluorescence (f = 2.0148). In another example, **7b**, the tetrazine-induced dark state is lower than the fluorophore's bright state by only 0.057 eV during vertical excitation (Fig. 8(d)). However, upon geometry relaxation in the excited state, the energy of the bright ICT becomes more stable than that of the dark state. This state-crossing could

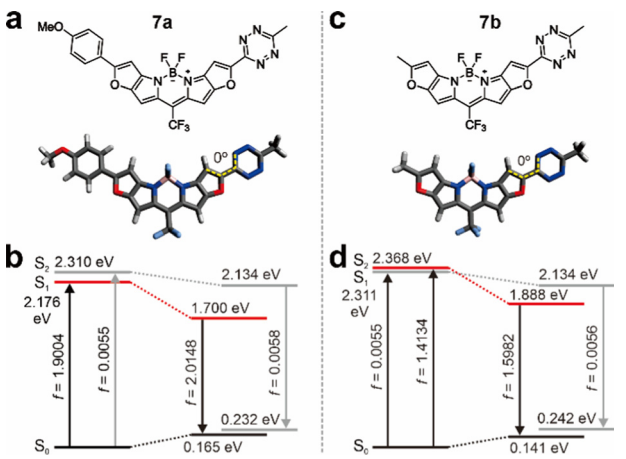

Fig. 8 Molecular structures, optimized geometries (a) and (c) and energy levels of key states during the excitation and de-excitation processes (b) and (d) of **7a** (left) and **7b** (right).

significantly compromise the quenching efficiency in **7b** and result in considerable background emissions. Although their products (**7a-BCN** and **7b-BCN**) upon the iEDDA reactions are highly emissive (Fig. S23, ESI†), strong background emissions in **7a** and **7b** would cause low FE ratios.

To circumvent this limitation of ICDS (and ETDS) in developing NIR fluorogenic dyes with excellent FE ratios, one may also incorporate other mechanisms, such as PET,[28,62,63] torsion-induced disaggregation (TIDA),[64] and twisted intramolecular charge transfer (TICT).[65–67]

Conclusions

In summary, we formalized an internal conversion to a dark state (ICDS) model to rationalize the fluorescence quenching mechanism in tetrazine-functionalized fluorogenic labels with integrated π-conjugations. In these labels, a low-lying dark state (n–π* transitions at the tetrazine moiety) resides below the bright state (π–π* transitions across the entire fluorophore, including the tetrazine fragment), activating the efficient internal conversion to the dark state and thus quenching the fluorescence. The subsequent iEDDA reaction destroys the tetrazine moiety and eliminates the corresponding dark state, turning on bright fluorescence. We noted that ICDS and a previously reported ETDS model demonstrated the opposite dependence on ΔE (the gap between the bright and dark states). Long-wavelength ICDS fluorophores with small ΔE tend to enhance internal conversions and thus afford much improved FE ratios compared to the ETDS-based labels (the small ΔE results in a low FE ratio). Inspired by the ICDS model, we summarized two design strategies for reducing ΔE, bathochromically shifting the spectra, improving the quenching/ICDS efficiency, and enhancing the fluorescence turn-on ratio *via* (1) expanding the π-conjugation and (2) exchanging the π-conjugation orders to induce quinoidization. We hope that this work could inspire the development of tetrazine-based fluorogenic labels with outstanding signal-to-noise ratios for many applications.

Author contributions

T. S.: conceptualization, methodology, investigation, formal analysis, visualization, data curation, writing – original draft, and writing – review and editing; W. Z.: investigation and funding acquisition; P. Y.: writing – review and editing; X. W. S.: project administration; X. L.: project administration, resources, fund acquisition, conceptualization, supervision, data curation, and writing – review and editing.

Conflicts of interest

There are no conflicts to declare.

Acknowledgements

This work was supported by the Ministry of Education Singapore (No. MOE-MOET2EP1020-0007), the Agency for Science, Technology and Research (A*STAR, Singapore; no. A2083c0051), and the National Natural Science Foundation of China (No. 12204229). The authors are grateful for the computational resources from the Singapore University of Technology and Design (SUTD) and the National Supercomputing Centre (NSCC, Singapore). T. S. acknowledges the scholarship support from the Doctor of Philosophy program at SUTD.

Notes and references

1 J. A. Prescher and C. R. Bertozzi, Chemistry in Living Systems, *Nat. Chem. Biol.*, 2005, **1**, 13–21.
2 D. M. Patterson, L. A. Nazarova and J. A. Prescher, Finding the Right (Bioorthogonal) Chemistry, *ACS Chem. Biol.*, 2014, **9**, 592–605.
3 N. K. Devaraj, The Future of Bioorthogonal Chemistry, *ACS Cent. Sci.*, 2018, **4**, 952–959.
4 R. K. Lim and Q. Lin, Bioorthogonal Chemistry: Recent Progress and Future Directions, *Chem. Commun.*, 2010, **46**, 1589–1600.
5 S. L. Scinto, D. A. Bilodeau, R. Hincapie, W. Lee, S. S. Nguyen, M. Xu, C. W. Am Ende, M. G. Finn, K. Lang, Q. Lin, J. P. Pezacki, J. A. Prescher, M. S. Robillard and J. M. Fox, Bioorthogonal Chemistry, *Nat. Rev. Methods Primers*, 2021, **1**, 30.
6 C. Qiu, Z. Cheng, C. Lv, R. Wang and F. Yu, Development of Bioorthogonal SERS Imaging Probe in Biological and Biomedical Applications, *Chin. Chem. Lett.*, 2021, **32**, 2369–2379.
7 Z. Shao, C. Zhang, X. Zhu, Y. Wang, W. Xu, Y. Chen, X. Wang, H. Zhu and Y. Liang, Design of a 1,8-Naphthalimide-Based Off-on Type Bioorthogonal Reagent for Fluorescent Imaging in Live Cells, *Chin. Chem. Lett.*, 2019, **30**, 2169–2172.
8 B. L. Oliveira, Z. Guo and G. J. L. Bernardes, Inverse Electron Demand Diels-Alder Reactions in Chemical Biology, *Chem. Soc. Rev.*, 2017, **46**, 4895–4950.
9 A. C. Knall and C. Slugovc, Inverse Electron Demand Diels-Alder (iEDDA)-Initiated Conjugation: A (High) Potential Click Chemistry Scheme, *Chem. Soc. Rev.*, 2013, **42**, 5131–5142.
10 M. L. Blackman, M. Royzen and J. M. Fox, Tetrazine Ligation: Fast Bioconjugation Based on Inverse-Electron-Demand Diels-Alder Reactivity, *J. Am. Chem. Soc.*, 2008, **130**, 13518–13519.
11 K. Lang and S. Mayer, Tetrazines in Inverse-Electron-Demand Diels-Alder Cycloadditions and Their Use in Biology, *Synthesis*, 2016, 830–848.
12 W. Chen, D. Wang, C. Dai, D. Hamelberg and B. Wang, Clicking 1,2,4,5-Tetrazine and Cyclooctynes with Tunable Reaction Rates, *Chem. Commun.*, 2012, **48**, 1736–1738.
13 T. Cañeque, S. Müller and R. Rodriguez, Visualizing Biologically Active Small Molecules in Cells Using Click Chemistry, *Nat. Rev. Chem.*, 2018, **2**, 202–215.
14 S. Liu, C. Lin, Y. Xu, H. Luo, L. Peng, X. Zeng, H. Zheng, P. R. Chen and P. Zou, A Far-Red Hybrid Voltage Indicator

Enabled by Bioorthogonal Engineering of Rhodopsin on Live Neurons, *Nat. Chem.*, 2021, **13**, 472–479.
15 T. Deb and R. M. Franzini, The Unique Bioorthogonal Chemistry of Isonitriles, *Synlett*, 2020, 938–944.
16 J. Tu, D. Svatunek, S. Parvez, H. J. Eckvahl, M. Xu, R. T. Peterson, K. N. Houk and R. M. Franzini, Isonitrile-Responsive and Bioorthogonally Removable Tetrazine Protecting Groups, *Chem. Sci.*, 2020, **11**, 169–179.
17 J. Sauer, D. K. Heldmann, J. Hetzenegger, J. Krauthan, H. Sichert and J. Schuster, 1,2,4,5-Tetrazine: Synthesis and Reactivity in [4+2] Cycloadditions, *Eur. J. Org. Chem.*, 1998, 2885–2896.
18 M. Wu, X. Wu, Y. Wang, L. Gu, J. You, H. Wu and P. Feng, Alkoxy Tetrazine Substitution at a Boron Center: A Strategy for Synthesizing Highly Fluorogenic Hydrophilic Probes, *ChemBioChem*, 2018, **19**, 530–534.
19 G. N. Lipunova, E. V. Nosova, G. V. Zyryanov, V. N. Charushin and O. N. Chupakhin, 1,2,4,5-Tetrazine Derivatives as Components and Precursors of Photo- and Electroactive Materials, *Org. Chem. Front.*, 2021, **8**, 5182–5205.
20 D. Kim, J. H. Lee, J. Y. Koo, H. M. Kim and S. B. Park, Two-Photon and Multicolor Fluorogenic Bioorthogonal Probes Based on Tetrazine-Conjugated Naphthalene Fluorophores, *Bioconjugate Chem.*, 2020, **31**, 1545–1550.
21 D. Wu and D. F. O'Shea, Fluorogenic NIR-Probes Based on 1,2,4,5-Tetrazine Substituted BF2-Azadipyrromethenes, *Chem. Commun.*, 2017, **53**, 10804–10807.
22 Z. Liu, Y. Zheng, T. Xie, Z. Chen, Z. Huang, Z. Ye and Y. Xiao, Clickable Rhodamine Spirolactam Based Spontaneously Blinking Probe for Super-Resolution Imaging, *Chin. Chem. Lett.*, 2021, **32**, 3862–3864.
23 Y. Wang, C. Zhang, H. Wu and P. Feng, Activation and Delivery of Tetrazine-Responsive Bioorthogonal Prodrugs, *Molecules*, 2020, **25**, 5640.
24 P. E. Z. Klier, A. M. M. Gest, J. G. Martin, R. Roo, M. X. Navarro, L. Lesiak, P. E. Deal, N. Dadina, J. Tyson, A. Schepartz and E. W. Miller, Bioorthogonal, Fluorogenic Targeting of Voltage-Sensitive Fluorophores for Visualizing Membrane Potential Dynamics in Cellular Organelles, *J. Am. Chem. Soc.*, 2022, **144**, 12138–12146.
25 P. Werther, K. Yserentant, F. Braun, N. Kaltwasser, C. Popp, M. Baalmann, D. P. Herten and R. Wombacher, Live-Cell Localization Microscopy with a Fluorogenic and Self-Blinking Tetrazine Probe, *Angew. Chem., Int. Ed.*, 2020, **59**, 804–810.
26 J. C. Carlson, L. G. Meimetis, S. A. Hilderbrand and R. Weissleder, BODIPY-Tetrazine Derivatives as Superbright Bioorthogonal Turn-on Probes, *Angew. Chem., Int. Ed.*, 2013, **52**, 6917–6920.
27 L. Chen, F. Li, M. Nandi, L. Huang, Z. Chen, J. Wei, W. Chi, X. Liu and J. Yang, Towards Tetrazine-Based Near-Infrared Fluorogenic Dyes: Is There a Wavelength Limit?, *Dyes Pigm.*, 2020, **177**, 108313.
28 W. Mao, W. Chi, X. He, C. Wang, X. Wang, H. Yang, X. Liu and H. Wu, Overcoming Spectral Dependence: A General Strategy for Developing Far-Red and Near-Infrared Ultra-Fluorogenic Tetrazine Bioorthogonal Probes, *Angew. Chem., Int. Ed.*, 2022, **61**, e202117386.
29 Y. Wang, G. Shen, J. Li, W. Mao, H. Sun, P. Feng and H. Wu, Bioorthogonal Cleavage of Tetrazine-Caged Ethers and Esters Triggered by Trans-Cyclooctene, *Org. Lett.*, 2022, **24**, 5293–5297.
30 N. K. Devaraj, S. Hilderbrand, R. Upadhyay, R. Mazitschek and R. Weissleder, Bioorthogonal Turn-on Probes for Imaging Small Molecules inside Living Cells, *Angew. Chem., Int. Ed.*, 2010, **49**, 2869–2872.
31 A. Wieczorek, P. Werther, J. Euchner and R. Wombacher, Green- to Far-Red-Emitting Fluorogenic Tetrazine Probes – Synthetic Access and No-Wash Protein Imaging inside Living Cells, *Chem. Sci.*, 2017, **8**, 1506–1510.
32 P. Werther, K. Yserentant, F. Braun, K. Grussmayer, V. Navikas, M. Yu, Z. Zhang, M. J. Ziegler, C. Mayer, A. J. Gralak, M. Busch, W. Chi, F. Rominger, A. Radenovic, X. Liu, E. A. Lemke, T. Buckup, D. P. Herten and R. Wombacher, Bio-Orthogonal Red and Far-Red Fluorogenic Probes for Wash-Free Live-Cell and Super-Resolution Microscopy, *ACS Cent. Sci.*, 2021, **7**, 1561–1571.
33 W. Chi, L. Huang, C. Wang, D. Tan, Z. Xu and X. Liu, A Unified Fluorescence Quenching Mechanism of Tetrazine-Based Fluorogenic Dyes: Energy Transfer to a Dark State, *Mater. Chem. Front.*, 2021, **5**, 7012–7021.
34 L. G. Meimetis, J. C. Carlson, R. J. Giedt, R. H. Kohler and R. Weissleder, Ultrafluorogenic Coumarin-Tetrazine Probes for Real-Time Biological Imaging, *Angew. Chem., Int. Ed.*, 2014, **53**, 7531–7534.
35 Y. Lee, W. Cho, J. Sung, E. Kim and S. B. Park, Monochromophoric Design Strategy for Tetrazine-Based Colorful Bioorthogonal Probes with a Single Fluorescent Core Skeleton, *J. Am. Chem. Soc.*, 2018, **140**, 974–983.
36 M. Bojtar, K. Nemeth, F. Domahidy, G. Knorr, A. Verkman, M. Kallay and P. Kele, Conditionally Activatable Visible-Light Photocages, *J. Am. Chem. Soc.*, 2020, **142**, 15164–15171.
37 W. Mao, J. Tang, L. Dai, X. He, J. Li, L. Cai, P. Liao, R. Jiang, J. Zhou and H. Wu, A General Strategy to Design Highly Fluorogenic Far-Red and Near-Infrared Tetrazine Bioorthogonal Probes, *Angew. Chem., Int. Ed.*, 2021, **60**, 2393–2397.
38 S. J. Siegl, J. Galeta, R. Dzijak, M. Dracinsky and M. Vrabel, Bioorthogonal Fluorescence Turn-on Labeling Based on Bicyclononyne-Tetrazine Cycloaddition Reactions That Form Pyridazine Products, *ChemPlusChem*, 2019, **84**, 493–497.
39 S. K. Choi, J. Kim and E. Kim, Overview of Syntheses and Molecular-Design Strategies for Tetrazine-Based Fluorogenic Probes, *Molecules*, 2021, **26**, 1868.
40 T. Förster, Energiewanderung und Fluoreszenz, *Naturwissenschaften*, 1946, **33**, 166–175.
41 D. L. Dexter, A Theory of Sensitized Luminescence in Solids, *J. Chem. Phys.*, 1953, **21**, 836–850.
42 S. Speiser, Photophysics and Mechanisms of Intramolecular Electronic Energy Transfer in Bichromophoric Molecular Systems: Solution and Supersonic Jet Studies, *Chem. Rev.*, 1996, **96**, 1953–1976.

43 X. Wu, D. Li, J. Li, W. Chi, X. Han, C. Wang, Z. Xu, J. Yin and X. Liu, Energy Transfer Followed by Electron Transfer (ETET) Endows a TPE-NBD Dyad with Enhanced Environmental Sensitivity, *Chin. Chem. Lett.*, 2021, **32**, 1937–1941.
44 N. Haase, A. Danos, C. Pflumm, P. Stachelek, W. Brutting and A. P. Monkman, Are the Rates of Dexter Transfer in TADF Hyperfluorescence Systems Optically Accessible?, *Mater. Horiz.*, 2021, **8**, 1805–1815.
45 R. B. Sekar and A. Periasamy, Fluorescence Resonance Energy Transfer (FRET) Microscopy Imaging of Live Cell Protein Localizations, *J. Cell Biol.*, 2003, **160**, 629–633.
46 T. Förster, Excitation Transfer and Internal Conversion, *Chem. Phys. Lett.*, 1971, **12**, 422–424.
47 M. Ricci, S. E. Bradforth, R. Jimenez and G. R. Fleming, Internal Conversion and Energy Transfer Dynamics of Spheroidene in Solution and in the LH-1 and LH-2 Light-Harvesting Complexes, *Chem. Phys. Lett.*, 1996, **259**, 381–390.
48 P. R. Callis, Binding Phenomena and Fluorescence Quenching. I: Descriptive Quantum Principles of Fluorescence Quenching Using a Supermolecule Approach, *J. Mol. Struct.*, 2014, **1077**, 14–21.
49 E. Hemmer, A. Benayas, F. Legare and F. Vetrone, Exploiting the Biological Windows: Current Perspectives on Fluorescent Bioprobes Emitting above 1000 nm, *Nanoscale Horiz.*, 2016, **1**, 168–184.
50 J. O. Escobedo, O. Rusin, S. Lim and R. M. Strongin, NIR Dyes for Bioimaging Applications, *Curr. Opin. Chem. Biol.*, 2010, **14**, 64–70.
51 X. Wu, D. Tan, Q. Qiao, W. Yin, Z. Xu and X. Liu, Molecular Origins of the Multi-Donor Strategy in Inducing Bathochromic Shifts and Enlarging Stokes Shifts of Fluorescent Proteins, *Phys. Chem. Chem. Phys.*, 2022, **24**, 15937–15944.
52 G. Hong, A. L. Antaris and H. Dai, Near-Infrared Fluorophores for Biomedical Imaging, *Nat. Biomed. Eng.*, 2017, **1**, 0010.
53 H. Li, H. Kim, F. Xu, J. Han, Q. Yao, J. Wang, K. Pu, X. Peng and J. Yoon, Activity-Based NIR Fluorescent Probes Based on the Versatile Hemicyanine Scaffold: Design Strategy, Biomedical Applications, and Outlook, *Chem. Soc. Rev.*, 2022, **51**, 1795–1835.
54 A. Tsuda and A. Osuka, Fully Conjugated Porphyrin Tapes with Electronic Absorption Bands That Reach into Infrared, *Science*, 2001, **293**, 79–82.
55 N. Wang, L. Zhan, S. Li, M. Shi, T.-K. Lau, X. Lu, R. Shikler, C.-Z. Li and H. Chen, Enhancement of Intra- and Inter-Molecular π-Conjugated Effects for a Non-Fullerene Acceptor to Achieve High-Efficiency Organic Solar Cells with an Extended Photoresponse Range and Optimized Morphology, *Mater. Chem. Front.*, 2018, **2**, 2006–2012.
56 M. M. Bai, H. V. Babu, V. Lakshmi and M. R. Rao, Structure–Property–Function Relationship of Fluorescent Conjugated Microporous Polymers, *Mater. Chem. Front.*, 2021, **5**, 2506–2551.
57 T. Shen, Y. Gao, C. Wang, Z. Xu and X. Liu, Methine-Quinoidal Fragment Induces Significant Bathochromic Shifts in Organic Dyes, *J. Phys. Chem. B*, 2021, **125**, 1447–1452.
58 S. Manzhos, Theoretical Analysis of the Solvatochromism of Organic Dyes Differing by the Conjugation Sequence, *J. Photonics Energy*, 2012, **2**, 028001.
59 S. Manzhos, H. Segawa and K. Yamashita, Computational Dye Design by Changing the Conjugation Order: Failure of LR-TDDFT to Predict Relative Excitation Energies in Organic Dyes Differing by the Position of the Methine Unit, *Chem. Phys. Lett.*, 2012, **527**, 51–56.
60 Y. Y. Tan, W. H. Tu and S. Manzhos, Computational Design of Small Organic Dyes with Strong Visible Absorption by Controlled Quinoidization of the Thiophene Unit, *Chem. Phys. Lett.*, 2014, **593**, 14–19.
61 K. Umezawa, Y. Nakamura, H. Makino, D. Citterio and K. Suzuki, Bright, Color-Tunable Fluorescent Dyes in the Visible-Near-Infrared Region, *J. Am. Chem. Soc.*, 2008, **130**, 1550–1551.
62 A. P. de Silva, T. S. Moody and G. D. Wright, Fluorescent PET (Photoinduced Electron Transfer) Sensors as Potent Analytical Tools, *Analyst*, 2009, **134**, 2385–2393.
63 Y. Koide, Y. Urano, K. Hanaoka, T. Terai and T. Nagano, Evolution of Group 14 Rhodamines as Platforms for Near-Infrared Fluorescence Probes Utilizing Photoinduced Electron Transfer, *ACS Chem. Biol.*, 2011, **6**, 600–608.
64 X. Zhang, J. Gao, Y. Tang, J. Yu, S. S. Liew, C. Qiao, Y. Cao, G. Liu, H. Fan, Y. Xia, J. Tian, K. Pu and Z. Wang, Bioorthogonally Activatable Cyanine Dye with Torsion-Induced Disaggregation for *in Vivo* Tumor Imaging, *Nat. Commun.*, 2022, **13**, 3513.
65 L. Chen, F. Li, Y. Li, J. Yang, Y. Li and B. He, Red-Emitting Fluorogenic BODIPY-Tetrazine Probes for Biological Imaging, *Chem. Commun.*, 2021, **58**, 298–301.
66 J. Galeta, R. Dzijak, J. Oboril, M. Dracinsky and M. Vrabel, A Systematic Study of Coumarin-Tetrazine Light-up Probes for Bioorthogonal Fluorescence Imaging, *Chem. – Eur. J.*, 2020, **26**, 9945–9953.
67 C. Wang, W. Chi, Q. Qiao, D. Tan, Z. Xu and X. Liu, Twisted Intramolecular Charge Transfer (TICT) and Twists Beyond TICT: From Mechanisms to Rational Designs of Bright and Sensitive Fluorophores, *Chem. Soc. Rev.*, 2021, **50**, 12656–12678.

